5th US Combustion Meeting
Organized by the Western States Section of the Combustion Institute
and Hosted by the University of California at San Diego
March 25-28, 2007.

Measurements of Hydrogen Syngas Flame Speeds at Elevated Pressures

M.P. Burke,[1] X. Qin,[1] Y. Ju,[1] and F.L. Dryer[1]

[1]Department of Mechanical and Aerospace Engineering, Princeton University, Princeton, New Jersey 08544, USA

Laminar flame speeds for syngas mixtures of various compositions up to 20 atm are measured with outwardly propagating spherical flames at constant pressure using more restrictive measures for data reduction that consider deviation from the ideal flow field caused by a non-spherical confinement. In the present paper, as in earlier high pressure study of flame speeds, a recently developed constant-pressure approach that utilizes a cylindrical test chamber is applied. For the first time, the effect of flow field on flame speed measurements is addressed in detail for these non-spherical constant-pressure chambers. The results from experiments and simplified analysis indicate that deviation from the assumed flow field causes significant errors in instantaneous flame speed measurement, which are amplified in the extrapolation to zero stretch rate. The relative deviation of the apparent flame speed from the true flame speed is found to scale with (σ-1) times the relative flow field deviation, where σ is the unburned to burned gas density ratio. This result demonstrates the significance of the flow field on the measured flame speed, since the density ratio typically assumes values of ~5-9 for hydrogen and hydrocarbon fuels in air. A simple model is developed to study the effect of flow disturbance in cylindrical confinements. In cylindrical chambers, where the flow is typically most constrained in the plane of measurement (radial direction), failure to consider this effect results in lower values for the measured flame speed.

Laminar flame speed measurements are reported for $H_2/CO/CO_2$ mixtures varying in equivalence ratio from 0.6 to 4.0, pressure from 1 to 20 atm, and CO_2 dilution from 0 to 25%. The corrected data range (0.6 cm < r < $0.30R_w$ where R_w is the chamber wall radius) is seen to raise the extrapolated burning velocity by as much as 6% from the burning velocity found from extrapolation over a wider range (0.6 cm < r < $0.54R_w$), which is more strongly influenced by flow field deviations. The experimental measurements are compared with experiments from McLean et al., Sun et al., and Hassan et al. (where applicable) and planar calculations using the kinetic mechanisms of Li et al., Davis et al., and Sun et al. While the experimental data and predictions for burning velocity agree reasonably well at lean conditions, large discrepancies occur at rich conditions. The substantial variation in the available stretch-corrected flame speed data indicate that significantly more data and more rigorous calculations of uncertainty are necessary before quantitative conclusions can be made and the performance of kinetic mechanisms can be properly assessed.

1. Introduction

The planar burning velocity is often termed a "fundamental combustion parameter," providing a measure of the coupled effects of exothermicity, diffusivity, and reactivity of a combustible mixture. It is the only flame speed unique to a gas of a fixed composition, initial temperature

and pressure, without further specification of hydrodynamic conditions, such as stretch rate, Reynolds number, extent of wrinkling, etc. The laminar flame speed serves as a useful input parameter for laminar flamelet calculations for turbulent combustion [1]. Not only does the burning velocity give information about the way a flame behaves under specific conditions, but it can be used to validate chemical kinetic and transport models. Consequently, the planar burning velocity is a frequently sought parameter in the combustion community, despite the fact that actual unstretched flames are rarely (if at all) encountered in applications and they are relatively difficult to measure.

Reliable experimental data and validated kinetic and transport models for H_2/CO combustion over a wide range of pressures, temperatures, compositions, and dilutions are necessary for the development of technology for coal-derived syngas combustion in stationary gas turbine engines as well as for solidifying the fundamental building block for modeling high-pressure, high-temperature hydrocarbon combustion. Burning synthetic gas is challenging in practice, because its diverse composition, consisting of CO, H_2, CO_2, H_2O, CH_4 and various trace species, can produce significant variations in combustion properties for different relative concentrations of its components. Therefore, kinetic mechanisms will be useful for predicting combustion characteristics of synthetic gas mixtures of all possible compositions and must be validated over a wide range of equivalence ratios, pressures, temperatures, and species concentrations. Since most practical applications including gas turbine engines perform at high pressures, reliable experimental data and validated models for high pressure conditions are especially important.

While a considerable amount of work on low pressure flame speeds for syngas mixtures has been performed [2-5], only one study has reported high pressure flame speeds [6]. Therefore, further investigation of laminar flame speeds for higher pressures typical of practical applications continues to be of interest.

The experimental method used in this study for flame speed measurement is the constant-pressure outwardly propagating spherical flame method. The spherical flame and counterflow flame methods are the two most common recently employed techniques, because their clearly defined stretch rates allow for extrapolation to an unstretched, adiabatic planar flame speed. New techniques have been developed to extend the spherical flame method to achieve measurements at pressures significantly higher than those used previously [7,8]. While flame speed measurements have previously been limited to pressures less than 10 atm, this method has allowed for stretch-corrected flame speed determination up to 60 atm [9].

The constant-pressure spherical flame method involves capturing schlieren pictures of a spherical flame and calculating the instantaneous flame speed and stretch from radius-time data [10,11]. Most studies employ the relations given by Strenlow and Savage [12] for an unconfined outwardly propagating spherical flame, in which the burned gas is assumed to come to rest after crossing the flame and the flame is taken to be infinitesimally thin,

$$s_u = \frac{\rho_b}{\rho_u} \cdot \frac{dr_f}{dt} \tag{1}$$

$$\kappa = \frac{2}{r_f} \cdot \frac{dr_f}{dt} \tag{2}$$

where s_u is the stretched flame speed, ρ_u and ρ_b the unburned and burned gas densities, r_f the flame radius, dr_f/dt the flame propagation speed, and κ the stretch rate. The density ratio is frequently computed by adiabatic calculation using the algorithm of Gordon and McBride [13], but in this study it is calculated in a planar flame calculation [14] using the mechanism of Li et al. [15]. Planar flame calculations using the mechanism of Davis et al. [16] yielded density ratios within 0.5% of those found using Li et al. for all cases studied. There are various methods found in the literature for relating the stretch rate and the stretched flame speed such that the fundamental mixture parameters, the unstretched burning velocity, s_u^o, and Markstein length, L_u, can be extracted as described in Ref. [17-21]. The present study employs the relation first postulated by Markstein [17]

$$s_u = s_u^o - L_u \cdot \kappa \tag{3}$$

derived from asymptotic theory for weakly stretched flames [22], but has been found to hold for more general conditions as discussed in Ref. [23].

Finally, the unstretched flame speed and the Markstein length can be extracted through a linear regression of (3). It should be mentioned that in stagnation and counterflow flame studies a nonlinear extrapolation method has been developed to relate the flame speed at the experimentally determined reference surface, the location of minimum velocity, to the flame speed at the theoretical reference surface, the location of 1% temperature rise [24]. As such, the nonlinear extrapolation approach has no bearing on spherical flame studies.

For the aforementioned spherical-flame theory to be satisfied exactly, it requires an unwrinkled, spherical, infinitesimally thin flame, which obeys the linear stretch relation, propagating in an unconfined environment with a constant density ratio across the front and no ignition, radiation or gravity effects. Of course, these assumptions are never satisfied exactly and, consequently, a large number of studies have been devoted to quantification and correction of the errors incurred by departures from the theoretical assumptions, including finite flame thickness [25], ignition disturbances [20,26], pressure rise [27-34], varying density ratio [18], radiation [2,18] and flame front wrinkling [35-37].

In the present paper, as in earlier high pressure study of flame speeds, a recently developed constant-pressure approach that utilizes a cylindrical test chamber is applied [7,8]. We describe departures of experimental results from expected behavior that cannot be explained by any of the above corrective analyses. We discovered the effect of a non-uniform flow field resulting from a non-spherical chamber, which has not been considered previously. While previous studies have mentioned the possibility of "wall interference" in these constant-pressure cylindrical bombs at large radii [9], this effect has not been qualitatively explained or quantitatively investigated. The motivation for investigating this effect in the present paper is that the cylindrical chamber geometry of the constant-pressure method used here and in earlier papers makes the presence of this particular effect more apparent, as shown below.

In the remainder of this paper, we will describe the experimental method, investigate the effects of flow field non-uniformity on the measurements, and report measurements on flame speed for syngas mixtures at high pressure with consideration of this effect.

2. Experimental Methods

The experiments are conducted in a dual-chambered, pressure-release type high-pressure combustion apparatus shown in Figure 1. The complete details of the experimental apparatus and procedure can be found in Ref. [8]. The chamber consists of two concentric cylindrical vessels of inner diameters 10 and 28 cm. The length of the inner chamber is 15.24 cm. Twelve holes of 2.2 cm in diameter are located in the lateral wall of the inner vessel to allow for pressure release. These holes are sealed with O-rings under the compression of the iron plates attracted by a series of permanent magnets imbedded in the wall. These iron plates can provide a seal between inner and outer chambers with a pressure difference above 0.3 atm. When the pressure difference vanishes or reverses, the iron plates open allowing the gas to flow from inner to outer chamber to maintain a constant pressure. Furthermore, since the volume of the inner vessel is 10 times smaller than that of the outer, the total pressure increase after combustion is small enough to ensure a constant pressure experiment and operational safety at high pressures.

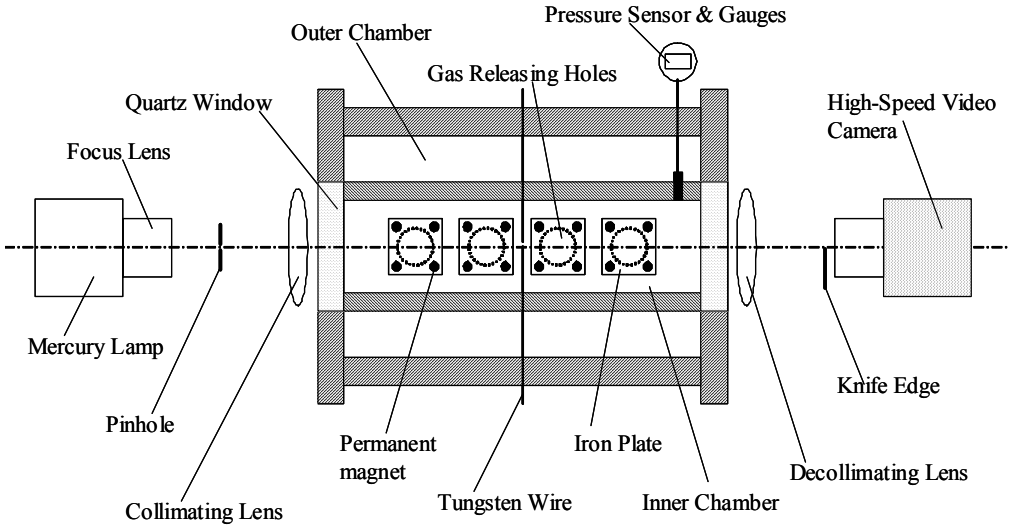

Figure 1: Schematic of pressure-release type cylindrical bomb and schlieren configuration

Schlieren photography is utilized for imaging the flame propagation. Light from a 100 W mercury lamp is focused on a 100 μm pinhole and collimated by a spherical lens. The collimated light passes through windows to the inner chamber and is focused on a horizontally installed knife edge. A high-speed digital video camera with 4 μs shutter speed and frame rate of 24,000 fps is used to record images of the propagating flame. From these images, the flame front is located and recorded using an automated detection program for ease of processing and reduction of human bias. The raw flame radius data are smoothed and flame front velocity calculated using local 2nd order polynomials fit by least-squares methods over a range of 3 mm surrounding each point. The data processed in this manner are consistent with the raw data as well as data processed through a more conventional local-averaging (low-pass) filter. The polynomial fitting is performed for each point over short spans of radius-time data, but not for the entire data set, which has been observed to produce false trends. The local polynomial processing is used to dampen any "end effects" of the regression analysis for stretch extrapolation and, more importantly, to aid in interpreting data observed in the experiment.

The plot of flame speed vs. stretch for a hydrogen-air mixture of equivalence ratio 3.0 at 1 atm shown in Figure 2a is indicative of the trend under the conditions used in this paper. There is a linear relation for large stretch (small radii), a change in curvature for moderate stretch (moderate radii), and a sharp slope for small stretch (large radii).

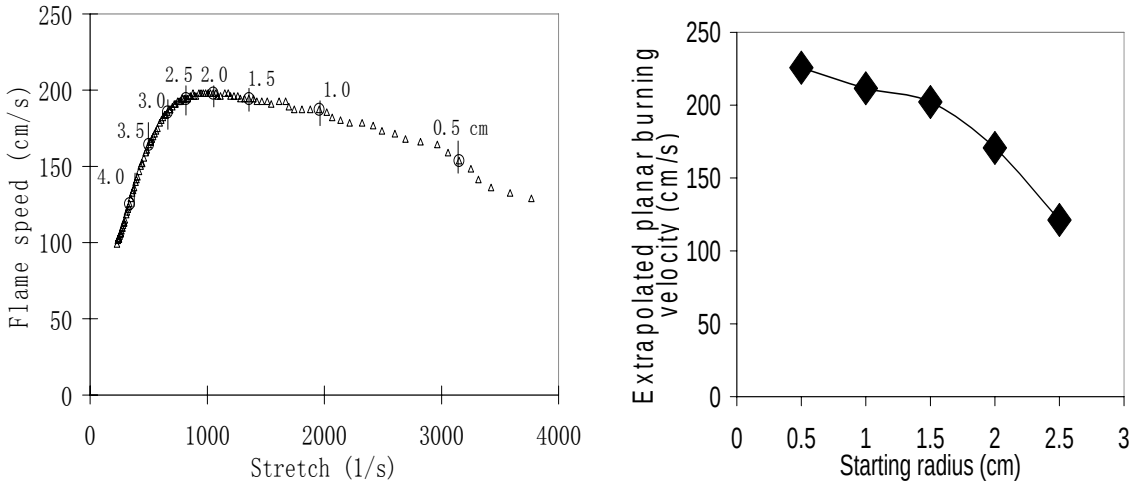

Figure 2: Exemplar experiment for a hydrogen-air mixture of equivalence ratio 3.0 at 1 atm

The resulting overall trend is not consistent with the theory used to extract planar values. However, none of the corrective analyses presented in the literature address this deviation. The same trend is observed when the inner chamber is open or closed to the outer chamber. In fact, the data used in this figure were taken when the iron plates were removed from the large holes connecting the inner and outer chambers. Therefore, the flame speed deviation in Figure 2 is clearly not caused by chamber pressure rise. Additionally, previous studies indicate the influence of radiation is small for these conditions [23]. Inspection of the schlieren movies reveals that the flame front image remains smooth and circular throughout its propagation. In fact, the flame speed has been observed to obey a linear relation with stretch rate in experiments [38] and in direct numerical simulations [34] under similar conditions.

It turns out that the above departure of observations and theory is caused by a deviation from the assumed flow field caused by the cylindrical chamber geometry. From Figure 2b, it is also clear that this effect has significant implications on determination of planar flame speeds (and Markstein lengths as well) and, as such, will be important to consider in spherical flame experiments. Figure 2b shows the unstretched flame speeds calculated through extrapolation to zero stretch over ranges of data that start at different radii and span 1 cm. For example, the extrapolated burning velocity for a starting radius of 0.5 cm is calculated by linear regression of flame speed vs. stretch data over the radius range from 0.5 to 1.5 cm, the extrapolated burning velocity for a starting radius of 1.0 cm is calculated over the radius range from 1.0 to 2.0 cm, and so on. In performing data reduction over ranges that include only flame radii less than half of the chamber radius, the extrapolated flame speed varies by 10%. This implies a significant limitation in the current methods used for constant-pressure cylindrical bombs and indicates the need for more restrictive data reduction and/or correction factors, or alternate experimental designs for high pressure flame speed determination.

3. Analysis of the Flow Field Effect

To demonstrate the sensitivity of flame speed measurement to flow field deviation, we will derive a relation between the relative deviation from the ideal flow field, $\delta = \Delta u/u$, and the relative deviation in instantaneous flame speed, $\varepsilon = \Delta s_u/s_u$. The rate of propagation of a premixed flame through a moving gas can be expressed as the sum of two components: the flame speed, s_u, relative to the gas in the direction normal to the flame front and the gas velocity, u_u, namely,

$$\frac{dr_f}{dt} = s_u + u_u \tag{4}$$

where the gas velocity has been taken in the direction normal to flame propagation for simplicity of presentation. Equation (4) gives the propagation rate as a function of the actual flame speed and gas speed. However, calculation of s_u under the assumption of an ideal flow field will yield an erroneous quantity for unburned flame speed, $s_{u,apparent}$, which is related to the apparent gas velocity, $u_{u,apparent}$, through

$$u_{u,apparent} = (\sigma - 1) \cdot s_{u,apparent} \tag{5}$$

by (1), where $\sigma = \rho_u/\rho_b$ is the unburned to burned gas density ratio. Therefore, these assumptions yield the expression,

$$\frac{dr_f}{dt} = s_{u,apparent} + u_{u,apparent} \tag{6}$$

By equating the two expressions for dr_f/dt, (4) and (6),

$$s_{u,apparent} + u_{u,apparent} = s_u + u_u \tag{7}$$

and expanding u_u for small deviation from the assumed flow field, Δu, using (5)

$$u_u = u_{u,apparent} + \Delta u = u_{u,apparent} + (\sigma - 1) \cdot s_u \cdot \delta \tag{8}$$

we can relate the deviation in the flow field, δ, to the deviation in the instantaneous flame speed, ε, through (7) and (8)

$$\varepsilon = \frac{s_{u,apparent} - s_u}{s_u} = (\sigma - 1) \cdot \delta \tag{9}$$

where the gas velocity deviation, δ, can found as a function of location for a given experiment using diagnostics or approximate flow field solutions. In situations where the deviation is small, such that the strength and spatial distribution of the hot gas expansion remains nearly constant, the flow velocity deviation, δ, is decoupled from the flame propagation process and is a merely a function of position relative to the boundary conditions. Thus, along the coordinate of dr_f/dt measurement, ξ, one can analytically or numerically solve $\delta = \delta(\xi)$, in which case the flow field deviation calculation for a given geometry has applicability for any mixture.

It is important to note from Equation (9) that an $O(1/(\sigma-1))$ deviation in the flow field will yield an O(1) error in the apparent instantaneous flame speed, which indicates more serious errors are incurred for mixtures with higher density ratios.

In physical terms, the outwardly propagating flame is a predominantly convective-driven phenomenon. Therefore, the quantity actually measured in the experiment, dr_f/dt, is (σ-1) times more sensitive to unburned gas velocity than the desired quantity, s_u, which is extracted from the dr_f/dt data. In extracting flame speeds from flame propagation rate data, care must be taken in general but especially with mixtures with large density ratios, e.g. near stoichiometric mixtures.

We will now formulate a simple model for the propagation of an outwardly propagating flame into an infinitely-long cylindrical pipe to illustrate the behavior of a propagating flame in a non-spherical chamber and develop an approximate model for the constant-pressure cylindrical bomb apparatus. The flow field model presented herein utilizes potential flow to simulate the unburned gas flow ahead of the flame produced by hot gas expansion with appropriate cylindrical pipe boundary conditions. While it should be noted that the actual flow is certainly not incompressible, a potential flow solution represents a simple way of recreating the flow produced by expansion of the combustion products in a given geometry. The following solution for the flow field is valid only for the unburned mixture, i.e. $r > r_f$.

Using solutions to Laplace's equation,

$$\nabla^2 \phi = 0 \tag{15}$$

the flow potential that satisfies the desired boundary conditions can be produced through a superposition of solutions. For small distortions of the flame, the flow created in the unburned gas by expansion of the burned gas can be represented as a source at the origin

$$\phi_{center} = \frac{m(t)}{4\pi \cdot \rho} \tag{16}$$

where m(t) is the time-varying strength and ρ is the radius from the origin. The strength of the source, m(t), is equal to the amount of mass displaced by thermal expansion per unit time,

$$m(t) = (\sigma - 1) \cdot 4\pi \cdot r_f^2 \cdot s_u . \tag{17}$$

The flame propagation of an unconfined spherical flame is then given by the vector form of (4)

$$\frac{d\underline{r}_f}{dt} = s_u \cdot \underline{n} + \underline{u}_u \tag{18}$$

where

$$\underline{u}_u = \nabla \phi . \tag{19}$$

The above relations using the flow potential given by (16) form a solution for a flame propagating into an unconfined environment. The apparent instantaneous flame speed is then calculated from dr_f/dt using the relations (18), (19), and (1). The model requires values for unstretched laminar flame speed, s_u^o, Markstein length, L_b, and density ratio, σ, as input parameters.

To create the cylindrical pipe boundary, we can superpose a ring of sources with strength distribution, q(t), at distance, η, from the origin summed over all angles, γ, from 0 to 2π,

$$\phi_{ring} = \int_0^{2\pi} \frac{q(t)}{\left\{[x - \eta \cdot \cos(\gamma)]^2 + [y - \eta \cdot \sin(\gamma)]^2 + z^2\right\}^{1/2}} \cdot d\gamma \tag{20}$$

where the strength distribution, q(t), and distance, η, are chosen to satisfy

$$u_r\big|_{r=Rw} = \left.\frac{\partial \phi_{cylinder}}{\partial r}\right|_{r=Rw} = 0 \tag{21}$$

where r is the radial direction in the pipe and R_w is the radius of the wall, and

$$\phi_{cylinder} = \phi_{ring} + \phi_{center}\,. \tag{22}$$

Likewise, the unburned gas velocity, $\underline{u}_u$, can be calculated by using the cylindrical flow potential of (22) in equation (19) and the apparent instantaneous flame speed, $s_{u,apparent}$, in a specific direction can be calculated using (18) and (1). The model is applicable when the flow deviation is small, such that the strength and spatial distribution of the hot gas expansion remains nearly constant, and the flow velocity deviation, δ, is decoupled from the flame propagation process and is a merely a function of flame position relative to the boundary conditions.

Figure 3a illustrates the effect of the cylindrical pipe on the apparent flame speed of a mixture with s_u^o = 225.7 cm/s, L_u = 0.0212 cm, and σ = 5.36, and R_w = 5 cm along the radial direction of propagation, which is the direction measured in cylindrical bombs. Of course, the true flame speed is unchanged, but determination of the flame speed from dr_f/dt, using the typical data reduction procedure for spherical flames described earlier, yields erroneous results for a flow field which departs from our assumptions.

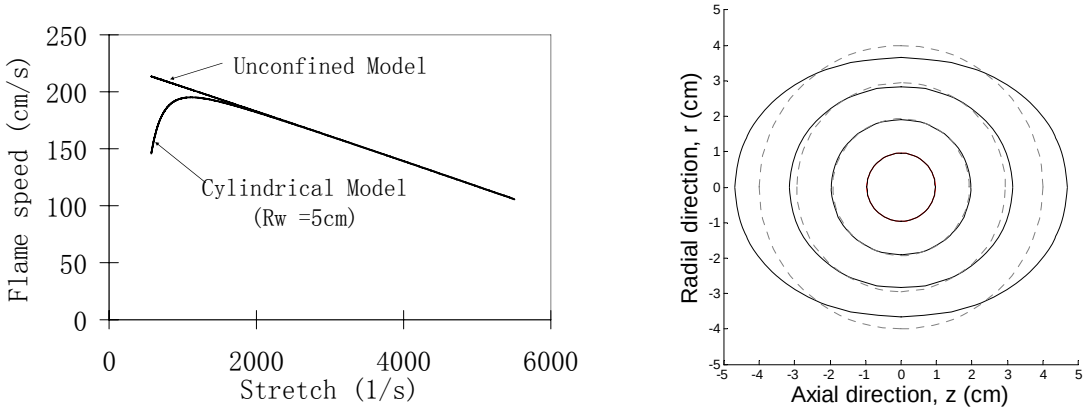

Figure 3: (a) Apparent instantaneous flame speed of unconfined and cylindrical models; (b) Flame shape evolution of unconfined (dotted) and cylindrical (solid) models

The plots reveal similarity of the unconfined and cylindrical cases for small radii (large stretch) and then a lower apparent flame speed for the cylindrical case for large radii (small stretch) due to a reduced unburned gas velocity in the radial direction. The linear region at small radii is thus the data range over which extrapolation should be performed.

Figure 3b displays the spatial evolution of the flame front for the unconfined and cylindrical pipe models, from the perspective perpendicular to the axial direction. The plot shows that the flame shapes for the two cases are similar for small radii, but then differ significantly for large radii. The cylindrical pipe compresses the wave front in the radial direction and stretches it in the axial direction forming an elliptical shape. In the perspective along the axial direction (the view

observed in schlieren pictures of the cylindrical-bomb experiments), the flame front for the cylindrical confinement is circular but progresses at a lower rate than that of the unconfined case.

It is expected that the flow in the cylindrical pipe may serve as an approximate model of the flow in a constant-pressure cylindrical bomb. Figure 4 compares the apparent flame speeds of an experiment of a hydrogen-air mixture of equivalence ratio 3.0 at 1 atm to the cylindrical pipe model using s_u^o = 225.7 cm/s, L_u = 0.0212 cm, and σ = 5.36 as before (where the values for s_u^o and L_u had been obtained from reduction of the experimental data over 0.5 cm to 1.5 cm). The agreement between the experiment and the cylindrical pipe model is quite good despite its simplicity. The apparent flame speed of both cases agree with the unconfined case for small radii (large stretch), diverge from the unconfined case at moderate radii (moderate stretch), and decrease rapidly at large radii (small stretch).

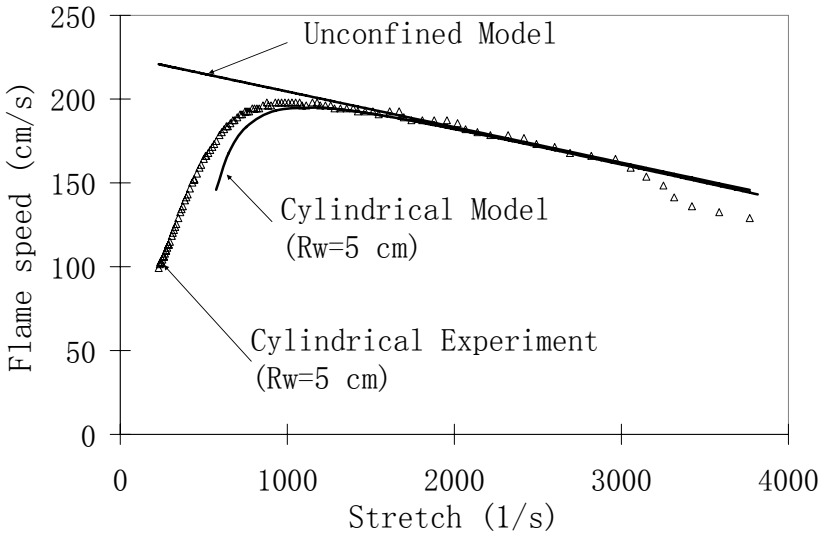

Figure 4: Comparison of cylindrical model to cylindrical experimental data

The result demonstrates the significance of flow field effects even in a constant-pressure combustion process. This marks the first time that the "wall interference" mentioned previously in the literature for cylindrical-bomb measurements has been qualitatively and quantitatively explained. The results from this analysis assist in the choice of data range and suggest possible correction factors for cylindrical bomb measurements.

4. Results and Discussion

Laminar flame speeds for syngas mixtures of various compositions up to 20 atm were measured using more restrictive measures for data reduction motivated by the results of the previous section. The syngas mixtures were composed of $\alpha_{CO2}CO_2 + (1-\alpha_{CO2})\alpha_{H2}H_2 + (1-\alpha_{CO2})(1-\alpha_{H2})CO$, where $\alpha_{CO2} = X_{CO2}/(X_{CO2}+X_{CO}+X_{H2})$ is the CO_2 molar fraction in the fuel mixture, $\alpha_{H2} = X_{H2}/(X_{H2}+X_{CO})$ is the H_2-CO ratio, and X is the mole fraction. The oxidizer mixtures were composed of $O_2+3.76N_2$ for air and O_2+7He for the oxygen-helium oxidizer. In light of the results from the flow field analysis section and previous studies of ignition effects [20,26], the data range used for extrapolation in this paper was $0.6 < r < 1.5$ cm ($= 0.30R_w$), in order to minimize the effect of ignition, transient processes and non-uniform flow field. During this range for the conditions studied here, the flame front image was observed to be relatively smooth

and circular and the stretched flame speed was observed to obey a linear dependence with stretch, as demonstrated in Figure 5a. Since flame speed measurements at low stretch rates are necessary for accurate extrapolation to zero stretch [39], the limitations imposed are expected to increase the uncertainty in the extrapolation compared to experiments that can accurately measure flame speeds at lower stretch rates.

Laminar burning velocities of an H_2-CO = 50:50 syngas mixture in air at 1 atm are presented from the present experiment in Figure 6, along with experiments by McLean et al. [2], Hassan et al.[3], and Sun et al. [6], and simulations using the recent mechanisms of Li et al. [15], Davis et al. [16], and Sun et al [6]. The measured burning velocities reach a peak value of 186 cm/s at an equivalence ratio of 2.0. Since the present experiments and those of Sun et al. were both conducted in constant-pressure cylindrical bombs, the difference in planar burning velocities results primarily from different choices of the data range used for extrapolation. For comparison, extrapolated planar burning velocities are presented in Figure 5b for flame speed-stretch data extrapolated over 0.6 cm < r < $0.30R_w$ and for data extrapolated over 0.6 cm < r < $0.54R_w$ (measurements were not made for flame radii larger than 2.7 cm in the experiment) along with the data of Sun et al. The corrected data range (0.6 cm < r < $0.30R_w$) is seen to raise the extrapolated burning velocity by as much as 6% from the burning velocity found from extrapolation over a wider range (0.6 cm < r < $0.54R_w$), which is more strongly influenced by flow field deviations.

While the deviation in the instantaneous flame speed is a function of density ratio and flame position only, the deviation in the extrapolated burning velocity is more complicated. The error in extrapolation also depends on $\Sigma(\kappa_i-\kappa_{mean})^2$ and κ_{mean}, where κ_i is the stretch rate at the i^{th} point and κ_{mean} is the mean stretch rate, as discussed in [39]. While Sun et al. did not report the data range used for these measurements specifically, they referred to Tse et al. [7] for a detailed description of the experiment, where the range r < $0.61R_w$ was used. The data of Sun et al. and the data extrapolated over 0.6 cm < r < $0.54R_w$ nearly coincide for equivalence ratio less than 2.0, but the data of Sun et al. are still lower at rich conditions. The difference in the values obtained using the two extrapolation ranges of the present experimental data demonstrates the significance of restricting data reduction to small radii in constant-pressure cylindrical bombs.

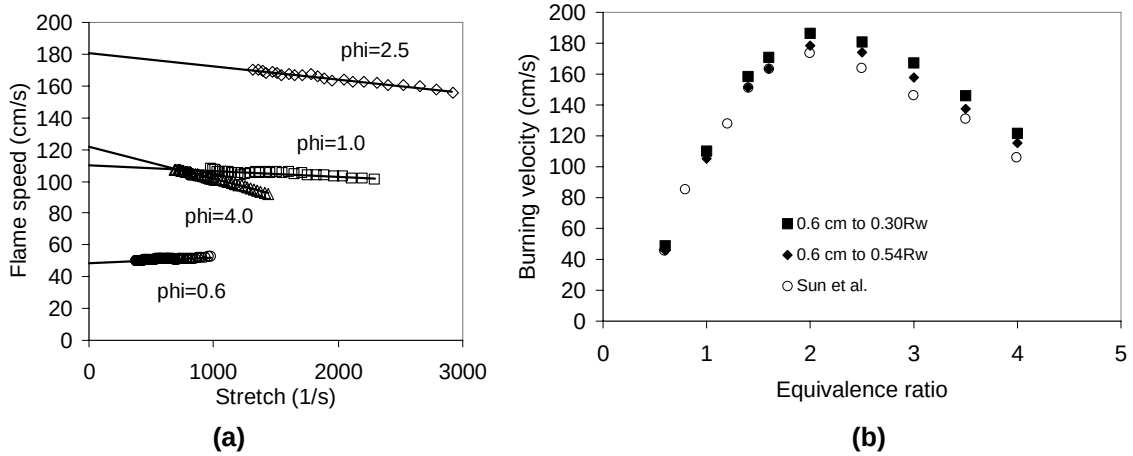

Figure 5: (a) Extrapolation of flame speeds to zero stretch rate using 0.6 cm < r < $0.30R_w$ and (b) comparison of laminar burning velocities using different data ranges for extrapolation for an H_2-CO = 50:50 syngas mixture in air at 1 atm

As Figure 6 shows, while the experiments and simulations are consistent for lean mixtures, the values diverge as the mixture becomes richer. Despite the fact that all four data sets were from stretch-corrected measurements of spherical flames, no two data sets agree well over the whole range of equivalence ratio and some differ by up to 40%. While Hassan et al. and McLean et al. report uncertainties (with 95% confidence) of 12% and 6%, respectively, these values differ by 40% at very rich conditions. The disagreement in the experimental data suggests that the uncertainties for flame speed measurements are much higher than previously suggested. Given the substantial variation in the data, significantly more data and more rigorous calculations of uncertainty for these experiments are necessary before quantitative conclusions can be gathered and the performance of these mechanisms can be properly assessed.

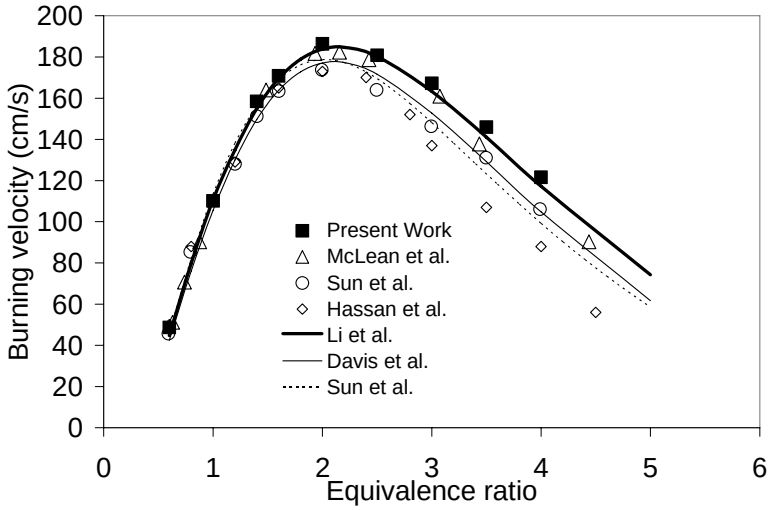

Figure 6: Laminar burning velocities for an H_2-CO = 50:50 syngas mixture in air at 1 atm

Laminar burning velocities over a range of equivalence ratios of an H_2-CO = 25:75 syngas mixture in oxygen-helium oxidizer for 10 and 20 atm are presented in Figure 7a. The measured burning velocities reach peak values of 106 cm/s at an equivalence ratio of 1.8 and 81 cm/s at an equivalence ratio of 1.6, for 10 and 20 atm, respectively. The present measurements are higher than those of Sun et al. at 10 atm by more than 10% at lean and stoichiometric conditions. They agree for most conditions at 20 atm, except for rich conditions where the present measurements are lower by more than 10%. Simulations using Li et al. and Sun et al. yield values within 5% of the present high-pressure measurements, except for rich conditions, where the present measurements indicate a stronger adverse dependence of flame speed with equivalence ratio than predicted by Sun et al. and Davis et al. at 20 atm and Li et al. at 10 and 20 atm.

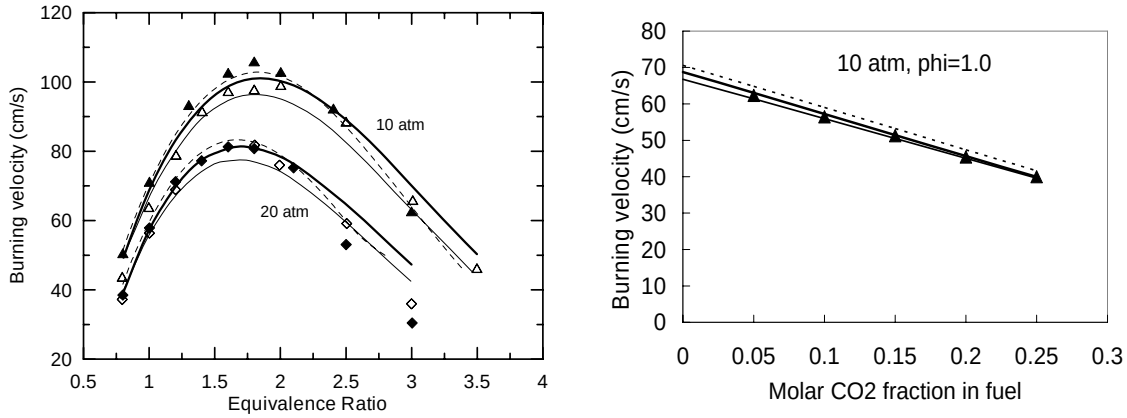

Figure 7: Laminar burning velocities at elevated pressures of an H_2-CO = 25:75 syngas mixture in an O_2:He = 1:7 oxidizer varying (a) equivalence ratio and (b) CO_2 concentration in the fuel mixture for equivalence ratio = 1.0 from present experiments (solid symbols), experiments by Sun et al. (open symbols), and simulations using Li et al. (bold lines), Davis et al. (solid lines), and Sun et al. (dashed lines)

Laminar burning velocities over a range of CO_2 concentrations of an H_2-CO = 25:75 syngas mixture in oxygen-helium oxidizer are presented in Figure 7b for 10 atm at stoichiometric conditions. The measured burning velocities indicate a decreasing linear dependence of burning velocity with CO_2 dilution. The experimental data for unstretched laminar burning velocity agree well with planar calculations using the three mechanisms for each CO_2 fraction as well as the decreasing linear slope in flame speed with increasing CO_2 dilution. The three mechanisms yield similar results, but Sun et al. predicts slightly higher flame speeds than Li et al., which predicts slightly higher flame speeds for low CO_2 concentrations and a slightly stronger adverse dependence of CO_2 concentration on the flame speed than Davis et al.

5. Concluding Remarks

The effect of flow field deviation due to constant-pressure non-spherical chambers is investigated experimentally and analytically, revealing that the resulting deviation in the measured instantaneous flame speed is (σ-1) times the deviation in the flow field, where σ is the unburned to burned gas density ratio. Since the density ratio for typical hydrocarbon-air mixtures is ~5-9, the flame speed measurement is extremely sensitive to departures from the theoretical flow field. A simple model is formulated to demonstrate the behavior observed in constant-pressure cylindrical bombs. In cylindrical chambers, where the flow is typically most constrained in the plane of measurement (radial direction), failure to consider this effect results in lower values for the measured flame speed. We plan to continue this work to quantify this effect more accurately for the constant-pressure cylindrical bomb with detailed simulations.

Planar burning velocities were measured for $H_2/CO/CO_2$ mixtures varying in equivalence ratio from 0.6 to 4.0, pressure from 1 to 20 atm, and CO_2 dilution from 0 to 25%. The data range used for extrapolation to zero stretch was chosen to be 0.6 cm < r < 1.5 cm (= $0.30R_w$), where R_w is the chamber wall radius, motivated by the results of the flow field analysis. The corrected data range (0.6 cm < r < $0.30R_w$) is seen to raise the extrapolated burning velocity by as much as 6% from the burning velocity found from extrapolation over a wider range (0.6 cm < r < $0.54R_w$),

which is more strongly influenced by flow field deviations. While the experimental data and predictions for burning velocity agree reasonably well at lean conditions, large discrepancies occur at rich conditions. Comparison of the available stretch-corrected flame speed data for the conditions studied reveals substantial variation, indicating that significantly more data and more rigorous calculations of uncertainty are necessary before quantitative conclusions can be made and the performance of kinetic mechanisms can be properly assessed.

Acknowledgments

The research at Princeton University was supported by the U. S. Department of Energy by grant #DE-FG26-06NT42716 and the Petroleum Research Fund from American Chemistry Society by grant PRF# 43460-AC5. We wish to thank Andrew Kelley of C.K. Law's group for helpful discussions and use of his flame front detection program and Marcos Chaos for his help with simulations and writing this paper.

References

[1] N. Peters, *Symposium (International) on Combustion* 21 (1986) 1231-1250.
[2] I.C. McLean, D.B. Smith and S.C. Taylor, *Symposium (International) on Combustion* 25 (1994) 749-757.
[3] M.I. Hassan, K.T. Aung, G.M. Faeth, *Journal of Propulsion and Power* 13 (1997) 239-245.
[4] C. M. Vagelopoulos, F. N. Egolfopoulos, *Symposium (International) on Combustion*, 25 (1994) 1317-1323.
[5] J. Natarajan, S. Nandula, T. Lieuwen, J. Seitzman, ASME Turbo Expo 2005, Reno-Tahoe, Nevada, June 6-9, 2005.
[6] H. Y. Sun, S. I. Yang, G. Jomaas, C. K. Law, *Proceedings of the Combustion Institute* 31 (2007) 439-446.
[7] S. D. Tse, D. L. Zhu, C. K. Law, *Proceedings of the Combustion Institute* 28 (2000) 1793-1800.
[8] X. Qin, Y. Ju, *Proceedings of the Combustion Institute* 30 (2005) 233-240.
[9] G. Rozenchan, D.L. Zhu, C.K. Law, S.D. Tse, *Proceedings of the Combustion Institute* 29 (2002) 1461-1469.
[10] S. Kwon, L.K. Tseng, G.M. Faeth, *Combustion and Flame* 90 (1992) 230-246.
[11] D. Bradley, R.A. Hicks, C.G. Lawes, G.W. Sheppard, R. Wooley, *Combustion and Flame* 115 (1998) 126-144.
[12] R.A. Strenlow, L.D. Savage, *Combustion and Flame* 31 (1978) 209-211.
[13] S. Gordon and B.J. McBride, *NASA Report No. SP-273* (1971).
[14] R.J. Kee, J. F. Grcar, M.D. Smooke, J. A. Miller, *Sandia Report* SAND 85-8240, 1993.
[15] J. Li, A. Kazakov, Z. Zhao, M. Chaos, F.L. Dryer, J.J. Scire, *International Journal of Chemical Kinetics* 39 (2007) 109-136.
[16] S.G. Davis, A. Joshi, H. Wang, and F.N. Egolfopoulos, *Proceedings of the Combustion Institute* 30 (2005) 1283-1292.
[17] G.H. Markstein, *Non-Steady Flame Propagation*. Pergamon, New York, 1964, p. 22.
[18] S.C. Taylor, *Burning Velocity and Stretch*, Ph.D. thesis, University of Leeds, Leeds UK, 1991.
[19] D.R. Dowdy, D.B. Smith, S.C. Taylor, A. Williams, *Symposium (International) on Combustion* 23 (1990) 325-332.
[20] D. Bradley, P.H. Gaskell, X.J.Gu, *Combustion and Flame* 104 (1996) 176-198.
[21] V.F. Karpov, A.N. Lipatnikov, P. Wolanski, *Combustion and Flame* 109 (1996) 436-448.
[22] P. Clavin, *Progress in Energy and Combustion Science* 11 (1985) 1-59.
[23] L. Qiao, C.H. Kim, G.M. Faeth, *Combustion and Flame* 143 (2005) 79-96.
[24] J.H. Tien, M. Matalon, *Combustion and Flame* 84 (1991) 238-248.
[25] L.K. Tseng, M.A. Ismail, G.M. Faeth, *Combustion and Flame 95* (1993) 410-426.
[26] S.Y. Liao, D.M. Jiang, J. Gao, Z.H. Huang, Q. Cheng, *Fuel* 83 (2004) 1281-1288.
[27] B. Lewis, G.J. Von Elbe, *Journal of Chemical Physics* 2 (1934) 283-290.
[28] D. Bradley, A. Mitcheson, *Combustion and Flame* 26 (1976) 201-217.
[29] P.G. Hill, J. Huang, *Combustion Science and Technology* 60 (1988) 17-30.
[30] D.A. Daly, J.M. Simmie, J. Würmel, N. Djebaili-Chaumeix, C.E. Paillard, *Combustion and Flame* 125 (2001) 1329-1340.

[31] K. Saeed, C.R. Stone, *Combustion and Flame* 139 (2004) 152-166.
[32] K. Takizawa, A. Takahashi, K. Tokuhashi, S. Kondo, A. Sekiya, *Combustion and Flame* 141 (2005) 298-307.
[33] F. Parsinejad, C. Arcari, H. Metghalchi, *Combustion Science and Technology* 178 (2006) 975-1000.
[34] Z. Chen, Y. Ju, 45th AIAA Aerospace Sciences Meeting and Exhibit, Reno, Nevada, Jan. 8-11, 2007.
[35] J.K. Bechtold, M. Matalon, *Combustion and Flame* 67 (1987) 77-90.
[36] O.C. Kwon, G. Rozenchan C.K. Law, *Proceedings of the Combustion Institute* 29 (2002) 1775-1784.
[37] C.K. Law, G. Jomaas, and J.K. Bechtold, *Proceedings of the Combustion Institute* 30 (2004) 159-167.
[38] K.T. Aung, M.I. Hassan, G.M. Faeth, *Combustion and Flame* 109 (1997) 1-24.
[39] Z. Zhao, A. Kazakov, J. Li, F.L. Dryer, *Combustion Science and Technology* 176 (2004) 1-19.